THE WAVEFIELD OF ACOUSTIC LOGGING IN MULTIPLE CASING MODELS

Hua Wang, Mike Fehler, Douglas Miller, Earth Resources Lab, MIT; Ioan Alexandru Merciu, Statoil ASA

This paper was prepared for presentation at the SPWLA 57th Annual Logging Symposium held in Reykjavik, Iceland June 25-29, 2016.

ABSTRACT

Successful operations for plug and abandonment (P&A) must seal the well bores to ensure that there is never leakage between geological horizons penetrated by the wellbore or to the surface. Acoustic logging methods for cement bonding, being designed for material evaluation of a single casing string, are currently unable to characterize cement and bonding of cement to casing when multiple concentric casing strings are present. When this is the situation, the inner pipes of the wells must be removed to leave only one layer of steel and cement that can be evaluated which increases the cost of the P&A. With the goal of improving the reliability of acoustic logging methods for material bonding evaluation in multiple casing bonding conditions, we use a 3D Finite Difference (3DFD) method to simulate wave propagation in cased borehole models including single casing and dual casing boreholes with different bonding conditions. Pressure snapshots for different models are shown which allow us to better understand the wave propagation. Data processing methods such as velocity-time semblance and dispersion analysis facilitate the identification of propagation modes in the different models. A modal decomposition method is also used in the data with an eccentered source. For single casing models, we assume that the basic formation modes can be easily discerned when the casing is well bonded. The P wave is submerged in the casing mode and the S wave has poor coherency when the cement is replaced with fluid. Acoustic logging tool with a monopole sonic source can be used for determine the bonding condition of different interfaces for the single casing model. For the dual casing models, it is easy to determine if there is good cement in both annuli and whether the outer casing is fully bonded by using monopole logging data. However, if the first annulus is not bonded well, the monopole data are not useful but it may be possible to use dipole or higher order modes to distinguish the bonding condition. The modal decomposition method for the data with an eccentered source helps us understand the higher order modes. New data processing methods and tool designs can be developed when we have a full understanding of the wavefield excited by an eccentered source.

INTRODUCTION

Well cementation, e.g. the pumping of cement into the annulus between the casing and rock or between two casings, is a key step of well completion to ensure well and formation integrity. A properly cemented well with low permeability cement (less than 0.1 mD) ensures good hydraulic isolation between reservoir layers and shallow aquifers (Lecampion et al., 2011), which can guarantee production efficiency as well as production and environmental safety (helping to avoid accidents such as the oil spill in the Gulf of Mexico in 2010). At the same time, the operations for plug and abandonment (P&A) of wells are becoming more and more important as the lives of many oil fields are coming to an end. P&A operations must seal the well bores to insure that there will never be leakage from the well structure to the surface or between the geological formations penetrated by the well. The cost of the P&A could be significantly reduced if a majority of the pipes in the hole can be left in place, especially in offshore environments there would be a great reduction of cost by using Light Well Intervention vessels. In this context, it is essential to accurately evaluate the material bonding in between and behind multiple casings with azimuthally resolved (3D) logging methods.

As a useful tool for determining cement bonding condition, acoustic logging methods for cement bonding analysis, which have typically been used during the well construction, are designed for

material evaluation behind a single casing string. However, it is hard to use the acoustic logging data to characterize cement and bonding of cement to casing when multiple concentric casing strings are present. The inner pipes of the wells must be removed to leave only one layer of steel and cement that can be evaluated. The removal greatly increases the cost of the P&A.

With the goal of improving the reliability of acoustic logging methods for material bonding evaluation in multiple casing bonding conditions, we use a 3D finite difference method (3DFD) to simulate the wavefield for multiple casing models with different bonding conditions.

We investigate the different modes propagating in the borehole by analysis of the full 3D wavefield records from 3DFD. By using data processing method we attempt to understand if we can identify fundamental mode propagation and the way that we can describe.

3DFD CODE AND CODE VALIDATION

Although analytical or semi-analytical methods can get an accuracy solution for some simple models, they cannot get the solutions for models with a complicated geometry. In this case we can only appeal to numerical methods such as 3DFD for assistant. We use the 3DFD code that has previously been used by Wang et al. (2015) to simulate wave propagation in boreholes with no or only a single casing string. The code uses a staggered grid and is second order in both space and time for considering the high impedance contrast between fluid and solid. Prior to using it, we must confirm its reliability for modeling situations where single or multiple steel casings are present in the model. We first investigate the case of sonic logging in a fluid-filled borehole (radius of 10 cm) surrounded by steel (An open hole model where the rock formation is replaced by steel).

We choose this model because it has high material contrasts and can be calculated easily using the Discrete Wavenumber integration method (DWM, Byun and Toksöz, 2003), which is a semi-analytical method and usually used for verifying the solution from the numerical method. Figure 1 shows the simulations obtained using both 3DFD and DWM. A grid size of 2 mm was used in the 3DFD code. Both the array waveforms (Figure 1a) and a single trace at 1.58 m offset (a random choice, shown in Figure 1b) show a nearly perfect match between the FD and DWM. The P, S, pR (pseudo Rayleigh), and ST (Stoneley) waves can be easily found with different lines marked according to their arrival times.

Table 1 Elastic parameter of media in the model.

Media	Vp (m/s)	Vs (m/s)	Density (kg/m^3)
fluid	1500	0	1000
Formation (sandstone)	4500	2650	2400
Steel	5500	3300	7850
Cement	3000	1730	1800

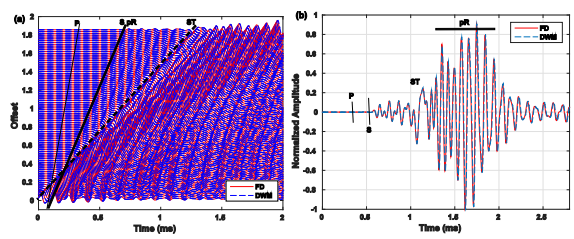

Fig.1 Comparison between the FD and DWM simulations for a model of an open hole surrounded by steel: (a) Array waveforms; (b) waveform on offset of 1.58 m.

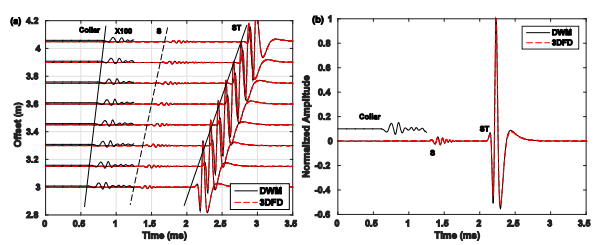

Fig.2 Comparison between the FD and DWM for an ALWD case: (a) Array waveforms; (b) waveform at offset of 3 m.

An acoustic Logging While Drilling (ALWD) model is one that contains typical large material

contrasts. We thus investigate the reliability of our 3DFD code to simulate an AWLD model. The model has a steel collar that is centralized in a fluid-filled borehole surrounded by rock. The geometry of a standard collar and borehole were chosen so that the inner- and outer- radii of the collar are 27 mm and 90 mm and the borehole radius is 117 mm, which correspond to a pipe with an ID of 1.06 inches and OD of 3.54 inches in a 4.6 inches borehole. A ring source is approximated by several point sources (Ricker wavelet of 10 kHz, which can cover the frequency band of the most common sonic logging tool) embedded on the collar. The full waveforms of the monopole LWD sonic tool simulated using 3DFD and DWM are shown in Figure 2. It can be seen that the FD result matches the result from the DWM very well. These validations give us confidence that the 3DFD code can successfully model a high impedance contrast cased hole that often challenges 3DFD codes.

SIMULATIONS FOR SINGLE CASING MODELS

Prior to investigating the wavefields in dual casing models, we need to understand the wavefields for the single casing model. Many studies have conducted for single casing models (e.g. Tubman et. al., 1984; Zhang et. al., 2013). Here we use our 3DFD simulator to investigate the full waveforms and wave propagation characteristics by examining wavefield snapshots for three different models: (1) casing immersed in fluid, (2) free casing in a borehole, and (3) perfect cement bonding between casing and formation.

Figure 3a shows side views of the borehole model with good cement between casing and formation. The color blue, red, light blue and orange are fluid, steel casing, cement and formation, respectively. For the casing immersed in a fluid model, the cement and formation are completely replaced with fluid and, only the cement is replaced with fluid for a free casing model (not shown here). The inner and outer radii of casing are 108 mm, and 122 mm and the radius of the borehole is 170 mm. In the simulations, the effect of the tool is ignored and a centralized point source with a 10 kHz Ricker wavelet is used. The pressure snapshots at 1.0 ms on a x-z profile are shown in Figures 3b (good bonded), 3c (free casing) and 3d (casing immersed in fluid). Figure 3d can help us understand the modes in the casing. An extensional casing mode is found at offsets of about 1.5 to 4 m while the ST wave follows and it leaks into both sides of the casing as a leaky mode (leaky-lamb S_0 mode, see Figure 4 in Wang et al., 2016). We use a dense receiver array with a 0.1 m interval to record the waveforms from the source position to the top of model along the z axis to understand the wave modes (as shown in Figure 4a). We find three visible modes as marked with lines. By extracting the dispersion curves (Wang et al., 2015) from the array waveforms, we find the three modes are the extensional casing mode (S0), ST and an additional ST (slow ST in Plona et al., 1992). Other modes including P, S, pR (pseudo Rayleigh) and ST modes are marked in Figures 3b and 3c. Although the wave front casing mode propagates as the fastest one in the pressure snapshots, the mode does not leak and is trapped in the casing when the casing is well cemented, which makes it invisible both in the borehole and formation (as shown in Figure 3b). The formation P and S waves are the first and second arrivals and can be obtained by an acoustic logging tool. However, the casing mode leaks into the fluid when the coupling is not good as seen in the free casing model shown in Figure 3c. In this situation, the first arrival in the borehole is the strong leaky casing mode and the formation P wave is submerged.

Figure 5 shows the array waveforms obtained from a centralized array receiver in the boreholes (displayed the same way as Figure 4a) and the related velocity analysis in the time (Kimball and Marzetta, 1986) and frequency domains. Figures 5a to 5c are for the well cemented cased hole. We see the waveforms having a time sequence of P, S, pR, ST and pR modes in Figure 5a. The waveforms at offset of 3 m to 3.7 m (interval of 0.1 m) are used for calculating velocity-time semblance (Figure 5b) and dispersion (Figure 5c). From the plots, we discern the P, S, and pR with multiple orders, and ST (poor coherency in Figure 5b) modes, respectively. The waveforms are very different when the cement is completely replaced with fluid and the wave modes in time sequence (Figure 5d) are casing, S that is not very coherent (Paillet and Cheng, 1991), ST, and the strongly dispersed pR (additional ST from the fluid between casing and formation being buried within the waveforms). The velocity plots in Figures 5e and 5f also show those modes. It is obvious that

there are two ST modes in Figure 5f corresponding to a ST inside the casing with a higher velocity and an additional ST in the fluid between casing and formation with a slower velocity.

The difference in the wavefield for the free casing and the well cemented cased boreholes shows a possibility for determining the bonding condition of different interfaces. By investigating the detail of the wavefields for the partially fluid-filled cement models with different thicknesses, we can get a direct method to determine the different bonding conditions including that between the casing outer interface and the borehole wall with data acquired by a most common array acoustic logging tool with a source having sonic frequencies (e.g. Zhang, et al., 2011).

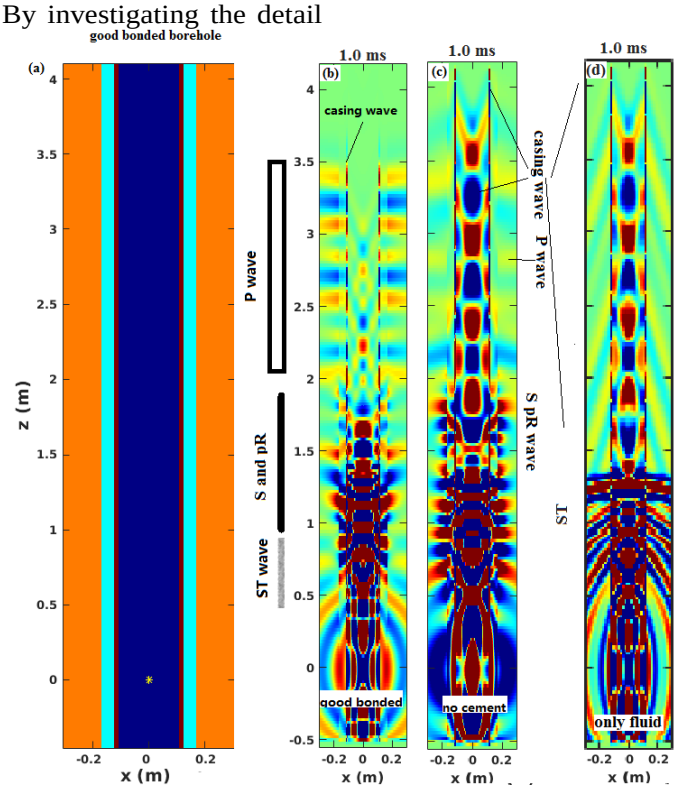

Fig.3 (a) X-Z profile of the model: A example for a single casing model in a cased hole (perfect cement boned model); the pressure snapshots for situations where the (b) cement is perfect bonded, (c) free casing and (d) casing immersed in fluid.

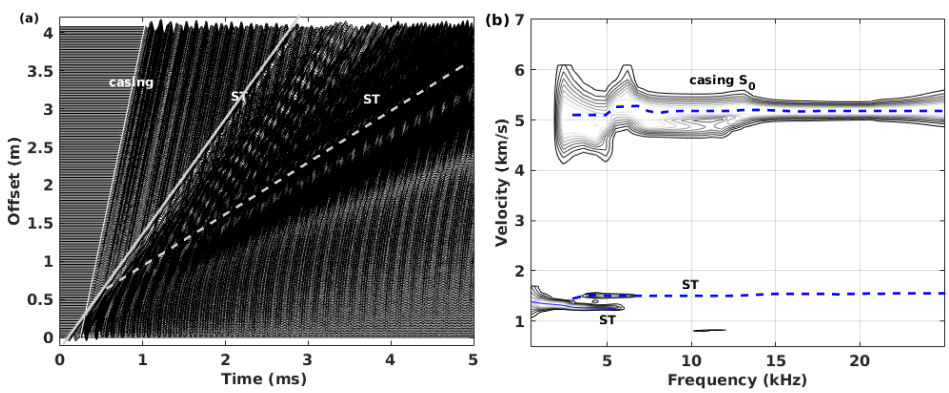

Fig.4 Waveforms acquired on a centralized receiver array for a centralized point source in a borehole with a casing that is surrounded by fluid.

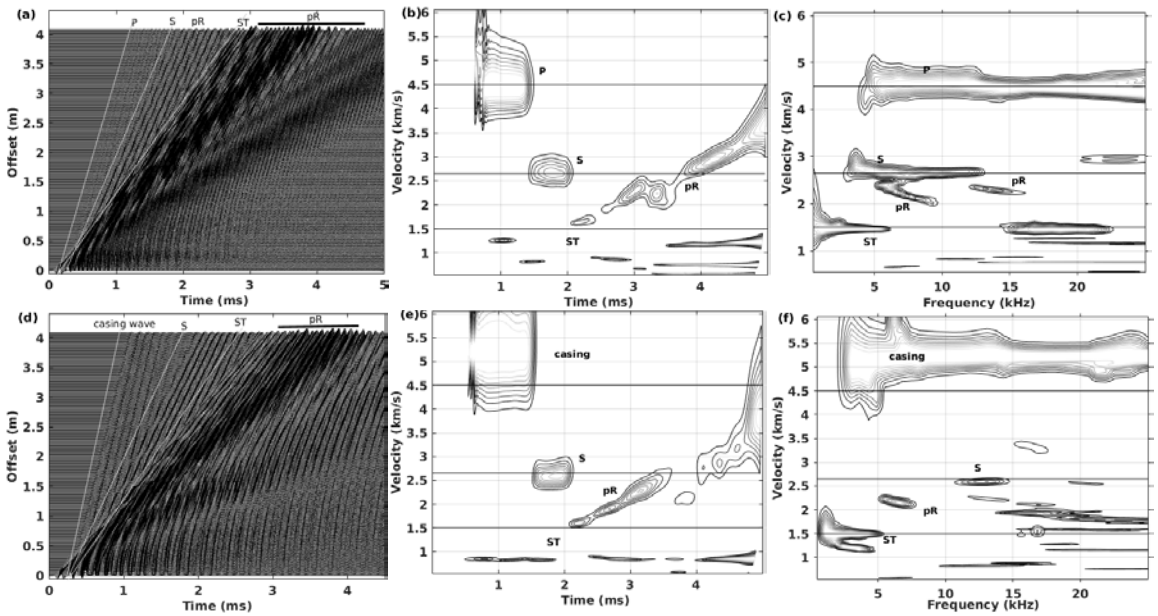

Fig.5 (a) Waveforms acquired in a well cemented cased hole with a centralized receiver array and a centralized point source located in the borehole fluid (b) time velocity plot, (c) frequency velocity plot. (d) – (f) are the same as (a)-(c) except for the case where cement completely is replaced with the fluid.

SIMULATIONS FOR DUAL CASING MODELS

As we discussed in the previous section, we can use sonic array logging data to determine the bonding condition of different interfaces when a single casing is present. However, it is not yet clear whether or not a sonic logging method can characterize cement and bonding of cement to casing when multiple concentric casing strings are present. Here we use the 3DFD method to investigate the wavefield in the dual casing models.

Using the 3DFD code, we have completed 8 simulations for borehole models with dual casing and we have stored the full 4 D waveform datasets. Table 2 gives a summary of the simulations. The geometry of the models are the same: the inner and outer radii are 108 mm, and 122 mm for the inner casing and 158 mm, 170 mm for the outer casing, respectively. The radius of the borehole is 206 mm. The inner annulus listed in Table 2 gives the space between the outer boundary of the inner casing and the inner boundary of the outer casing. The outer annulus is the distance between the outer boundary of the outer casing and the formation.

1) Centralized point source cases

Figure 6 shows a side-view for a dual casing model (Model 1 in Table 2) and wavefield pressure snapshots (x-z profiles) for different models (Models 1 to 4 in Table 2) at 1 ms. Color codes in Figure 6a for different media are the same as those in Figure 3a. A centralized point source located at the star was used. In the Figure 6b, the terms c and f at the top of the plots indicate whether there is cement or fluid in the first and second annuli (Refer to Table 2). The ranges where different modes appear in the different cases are also marked. The casing wave, marked with the white bar ranges from 2.3 to 4 m in both the 1f2f and 1f2c models, is an extensional mode (only one color in the same z location in the casing). However, the amplitude of the casing wave in 1c2c is very small (marked with a dashed rectangle) and cannot leak into the borehole and formation due to the good coupling between casings, cements and formation. The P and S waves are very clear in this situation, but they cannot be seen in the other 3 models. The difference in the wavefields shown for 1f2f and 1f2c is very small and can only be found in the range of the ST wave marked with a solid rectangle. For the 1c2f, the leakage of wave

propagating in first casing and the cement in the first annulus is the first arrival in the borehole.

Figures 7 to 11 show the waveforms, velocity-time semblance plots, and dispersion plots for the four different models. The formation P and S waves are very clear in Figure 7a and we can obtain the velocity from the velocity-time semblance plot (Figure 7b). The dispersion plot in Figure 7c shows the pR wave with multiple orders. The coherence of the ST wave is not clear in Figure 7b due to the interference with the strong dispersive pR wave. Combined with the waveforms in Figure 5a, we find that if the casing is well boned with cement even for a dual casing model, it is very easy to obtain the formation waveforms from the borehole logging tool.

For the 1c2f, the cement in the second annulus is completely replaced with fluid. The waveforms in Figure 8a look a bit different from those in Figure 7a. A newly appearing mode (marked by a solid gray line) makes the formation P wave hard to see. The velocity obtained from the semblance plot in Figure 8b for this mode is a bit lower than 5000 m/s, which is lower than the velocity of the casing mode in Figures 4b and 5e. The dispersion curve shown in Figure 8b is also different from that shown in Figure 5f although they are look similar. We will discuss this in the following by comparing the first arrival times for the different models.

Although the S and ST waves can be seen in Figure 8a, the coherence of the S wave is not good which leads to an estimation of velocity (Figure 8b) that is slight slower than that of the formation S wave. The dispersion curve for the ST mode shows there are two ST modes in the waveforms which is similar to the free single casing model in Figure 5f: the fast one is the borehole ST wave and the slow one is the additional ST (marked with a black solid line in Figure 8a) in the second fluid annulus.

Table 2 simulations for dual casing models

Simulation Number (name)	Inner annulus	Outer annulus	Source
1 (1f2f)	Fluid	Fluid	Centralized point source
2 (1f2c)	Fluid	Cement	same as above
3 (1c2f)	Cement	Fluid	same as above
4 (1c2c)	Cement	Cement	same as above
5 (1f2f)	Fluid	Fluid	Eccentered point source
6(1f2c)	Fluid	Cement	same as above
7(1c2f)	Cement	Fluid	same as above
8(1c2c)	Cement	Cement	same as above

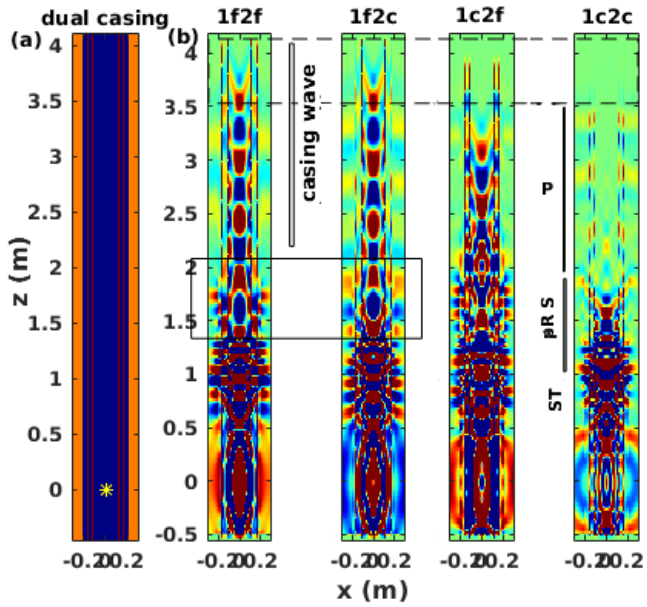

Fig.6 Side-view for a dual casing model (Model 1 in Table 2) and wavefield pressure snapshots (x-z profiles) for different models at 1 ms. Model names are given at the top of each plot and refer to those listed in Table 1.

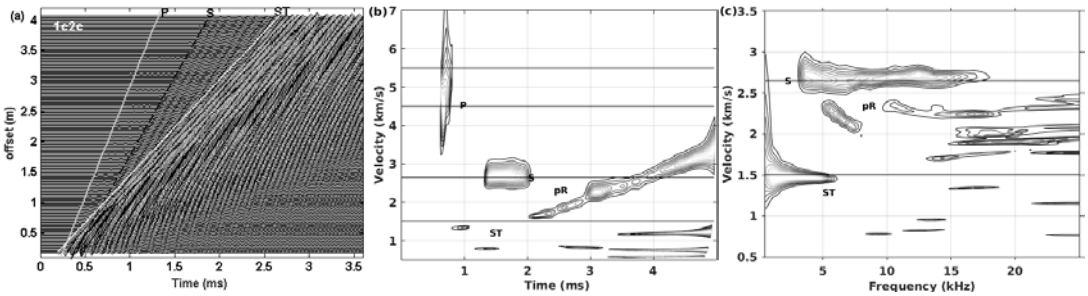

Fig.7 Waveforms acquired in a well cemented bonded cased hole (1c2c) using a centralized receiver array with a centralized point source in the borehole fluid.

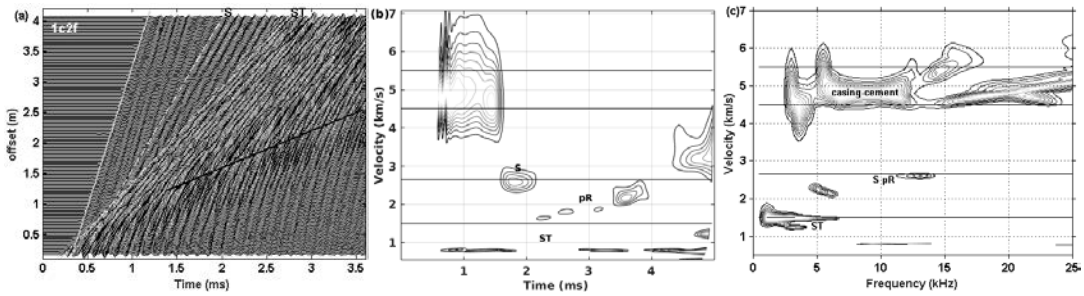

Fig.8 Waveforms acquired in model 3 (1c2f) by a centralized receiver array with a centralized point source in the borehole fluid

As a direct comparison, Figure 9 shows the waveforms and velocity analysis for model 2 (1f2c). The waveforms in Figure 9a are different from those in Figure 8a and both the P and S wave cannot be picked. The result from the free single casing model can be used as a reference. According the velocity-time semblance plot (Figure 9b) and dispersion curves (Figure 9c), we

can identify the first wave marked with a gray solid line as a casing wave propagating in the first case and the waveforms marked with a dash line indicate a ST wave. Between these two waveforms, the pR wave with strong dispersion leads poor coherence of the S wave which means that the S wave cannot be seen. There are two ST waves found in the dispersion analysis, which are identified as the borehole ST wave and an additional ST wave (marked with a black line in Figure 9a) in the first fluid annulus.

For the worst case, shown in Figure 10, the cement in the two annuli is completely replaced with fluid (Model 1 in Table 2). It is very hard to find differences between Figures 9 and 10 because most energy is trapped in the borehole once the first annulus is replaced with fluid no matter the what material is in the second annulus. A difference can be found in the later part of the waveforms marked with a white rectangle in the figures, which results from the third ST wave in the second annulus. Therefore it is necessary to utilize the later part of the waveforms to evaluate the presence of cement. However, with limited receivers having sparse sampling in a commercial array logging tool these later phases could not be distinguished.

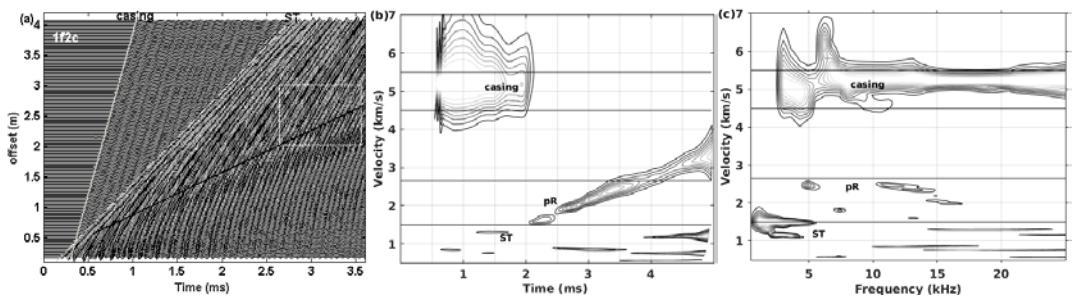

Fig.9 Waveforms acquired in model 2 (1f2c) by a centralized receiver array with a centralized point source in the borehole fluid.

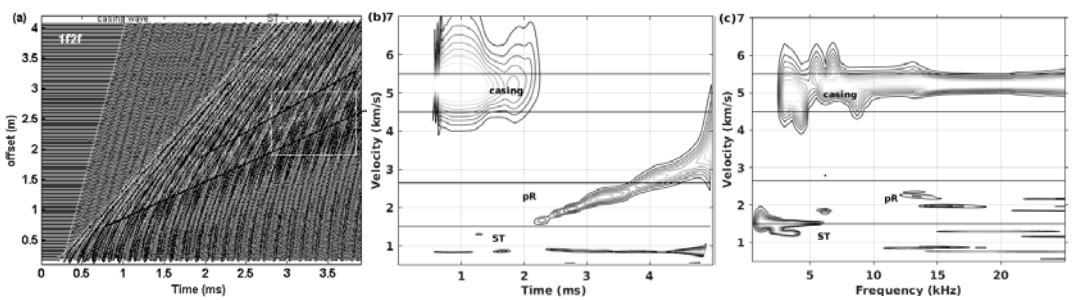

Fig.10 Waveforms acquired in a free casing hole (Model 1, 1f2f) by a centralized receiver array with a centralized point source in the borehole fluid.

To compare the waveforms for different models, we plot traces at 3 m offset (position of the first receive for a most common array tool) for different models in Figure 11. All the waveforms are normalized by the amplitude of the waveform obtained for model 1c2c. We use the black solid and dash-dot lines to indicate the arrival time of casing and P waves, respectively. It is clear that the casing waves are the first arrivals in the 1f2f and 1f2c cases and P wave are an obvious first arrival for model 1c2c. The time of the first arrival in 1c2f (marked with a dash line) is between the arrival time of the casing and P waves, which is similar as the case of partial cement in the second bonded interface in a single casing model (e.g. Zhang, 2011). The arrival time of the S wave is marked with a gray solid line and is only obvious in case 1c2c. Although an obvious wave follows the casing-cement mode in 1c2f and has a recognizable arrival time, it is later than the arrival time of the S wave corresponding to the obtained slower S velocity in Figure 8b. A difference in the waveforms marked with a rectangle indicates the additional ST waves, which can be used for distinguishing the 1f2f and 1f2c.

We conclude that one can easily distinguish 1c2c, 1c2f from the other two models by the first arrival times. We need to use the later part the waveforms after the arrival time of the borehole ST wave to distinguish the 1f2f

and 1f2c models. However, wave extraction from the later part of the waveforms in field data would challenge data processing methods because of the limited number of receivers having sparse sampling.

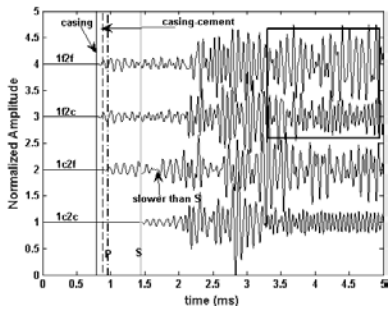

Fig.11 Waveforms acquired in different models at 3 m offset.

2) Eccentered point source cases

In the previous section, we discussed different dual-casing models with a centralized point source. For all the sonic logging, the rule for logging is to keep the sources centralized in the borehole. However, if the logging operation is carried out in multiple casings and eccentered outer casings will also makes the source eccentered even the source is centralized in the inner casing. The complexity will rise from the fact that the symmetry is broken. Here we will discuss an eccentered point source for those four models because the rich multipole modes can be excited when the symmetrical wavefield is broken by an eccentered point source. With these modeling, we can understand the fundamentals of wave propagation in the multiple casing models.

Figures 12 to 15 show the pressure snapshots at 1 ms of different profiles for the four different models. The side views (x-z profile) of the models for 1c2c, 1c2f, 1f2c, and 1f2f are shown in the panel (a) in each figure. The color codes for the models are same as Figure 3a. The offset of the point source (marked with star in the figures) from the borehole axis is 46 mm along the x axis, which is the radius of the most common downhole sonic tool. Because the source is eccentered in the x direction, the snapshots in y-z profiles (in the panel c in the figures) are same as those in the centralized point source cases, which be used as a reference for discern modes in the snapshots of the x-z profiles. According to the time sequence of the waves seen in the profiles, we find apparent multipole modes beginning from about the S wave in 1c2c (Figure 12b), casing-cement wave in 1c2f (Figure 13b), casing wave in 1f2c (Figure 14b) and 1f2f (Figure 15b) due to the broken symmetry of the pressure wavefield in x-z profiles.

For the x-y profiles, panels d, e, and f in each figure, there are 5 white circles with different diameters. The inner 2 circles are the inner casing, and the circle with the largest diameter is the borehole wall. The other two circles are for the outer casing. For all the simulations, there are two different colors in the casing along the x direction in the pressure snapshots in x-y profiles indicating that the anti-symmetric modes introduced (Modes A series in Wang et al., 2016). In addition, multipole modes can be also found in the borehole fluid.

In figures 14b and 15b, we find a distinct difference in the x-z profile pressure snapshots between 1f2c and 1f2f, where the eccentered source makes them different from the casing wave. This indicates the excitation of the multiple modes is dependent on the presence of fluid or cement and we can use the multiple modes to help us determine the bonding condition for 1f2c and 1f2f.

To investigate the mode generation, we apply a modal decomposition method to the wavefields found for an eccentered point source. We use the method of Chen et al. (2010) to extract the multipole modes. The extracted monopole and dipole modes for different models are shown in Figures 16 and 17. The P wave in Figure 16 is zoomed in. Comparing the extracted monopole waveforms (Figure 16) with the recorded data in the centralized source cases (Figures 7a, 8a, 9a, and 10a), we find that they are almost the same and only small difference appears in the ST wave for 1c2c, and the S waves in 1f2c and 1f2c. The reason for the slight difference is due to the different excitation of the monopole mode at the two source positions. As we discussed, we can use the monopole data to distinguish the 1c2c and 1c2f models, but we cannot use the data to distinguish the other two models.

Like Figure 16a, the P wave in Figure 17a is zoomed in for easy evaluation. The flexural modes dominate the waveforms for the models and the four figures (Figures 17a to 17d) look quite different from each other, especially for the 1f2c and 1f2f cases, in which the waveforms exhibit a difference in the modes following the casing mode. Although the waveforms at 3 m offset in the extracted dipole waveforms, shown in Figure 17e, for the 4 different models look similar to those in Figure 11, the strong flexural modes make strong differences in waveforms among the 4 models that is visible especially for the rectangular region highlighted for 1f2f and 1f2c models.

By comparing modes excited for different models, we have found large differences and this gives us confidence that further study will allow us to identify approaches for using a sonic tool to determine the bonding condition in a dual casing model.

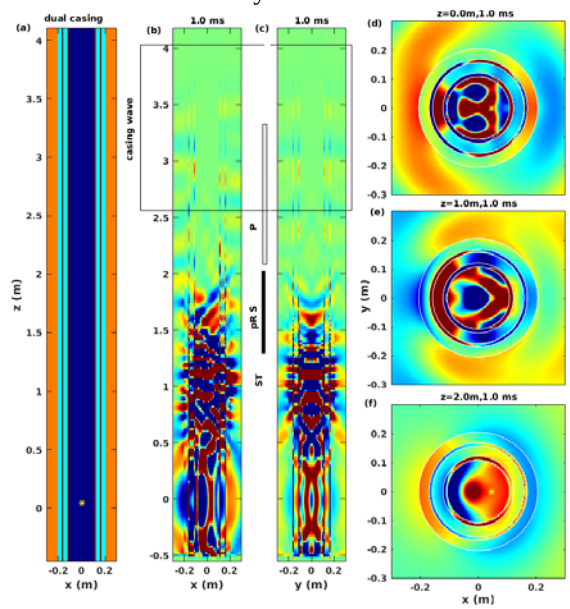

Fig.12 A well bonded dual casing borehole model (1c2c) and snapshots of the pressure wavefield at 1 ms for different profiles.

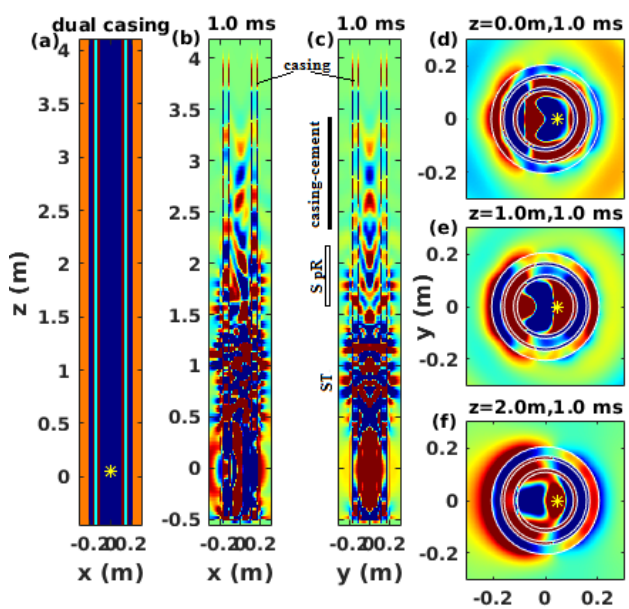

Fig.13 A dual casing borehole model (1c2f) with cement in the second annulus being totally replaced with fluid and snapshots of the pressure wavefield at 1 ms for different profiles.

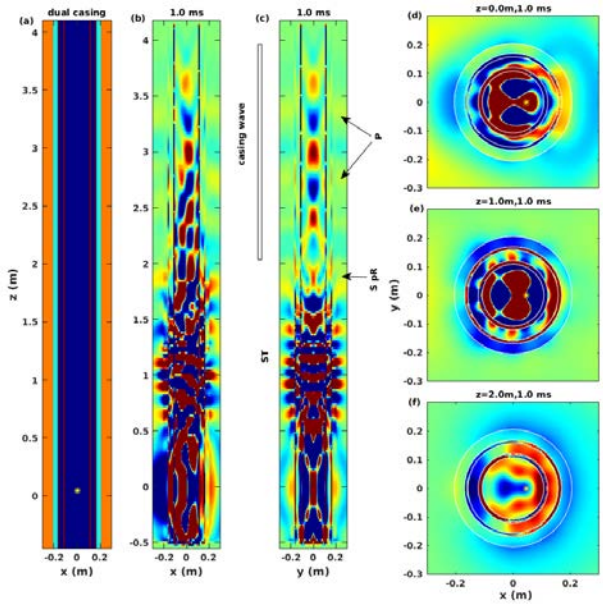

Fig.14 A dual casing borehole model (1f2c) with cement in the first annulus being replaced with fluid and snapshots of the pressure wavefield at 1 ms for different profiles.

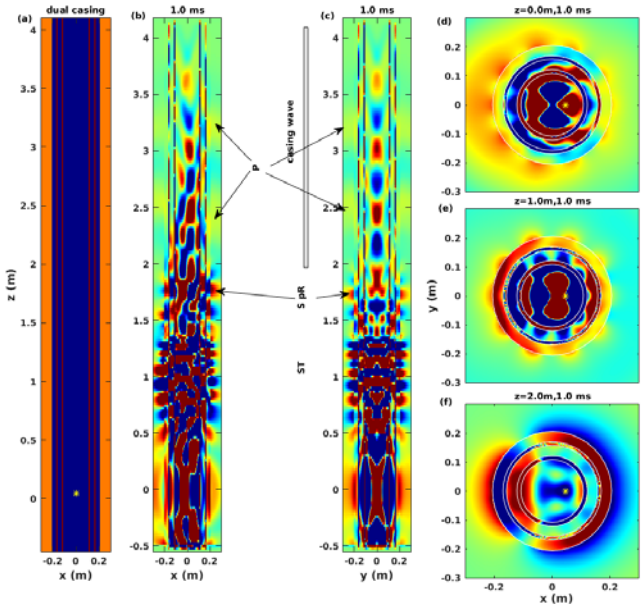

Fig.15 A dual casing borehole model (1f2f) with cement in both annuli being replaced with fluid and snapshots of the pressure wavefield at 1 ms for different profiles.

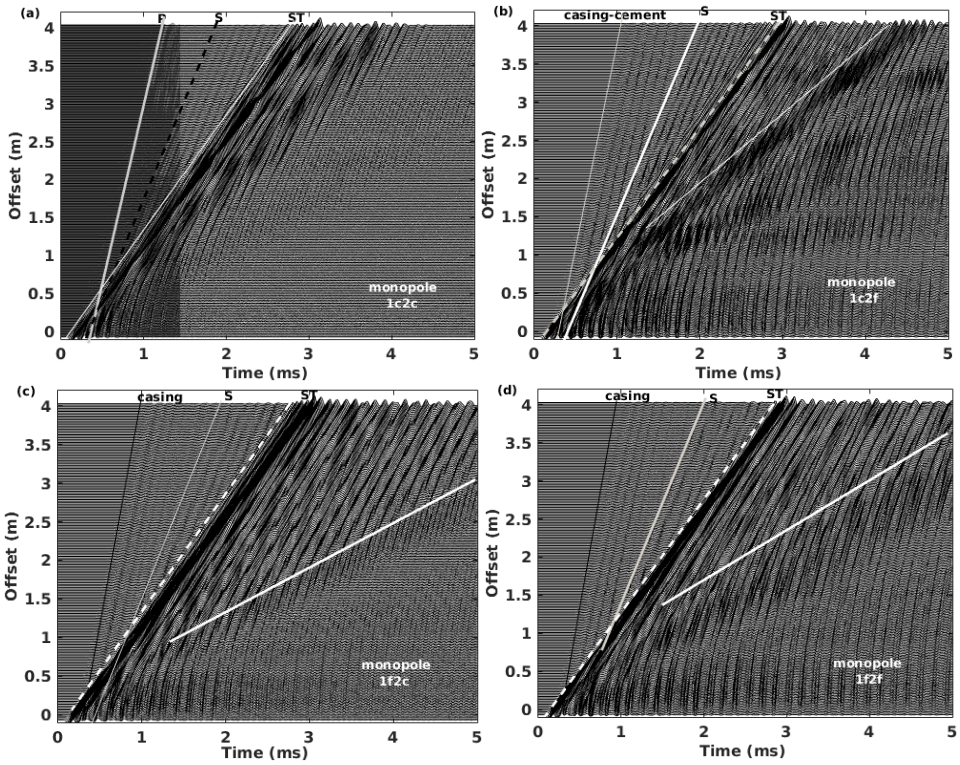

Fig.16 Monopole modes extracted from the data for different models with an off-center point source. The P wave in (a) is zoomed due to its small amplitude.

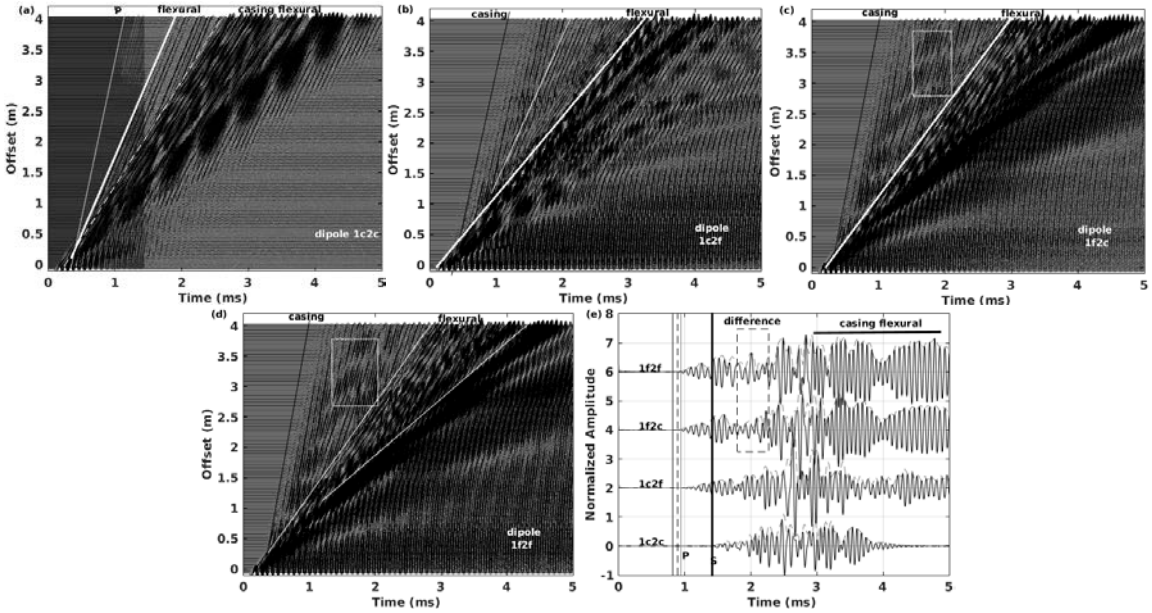

Fig.17 Dipole modes extracted from the data for different models with an off-center point source.

CONCLUSIONS

We have used a 3DFD method to simulate wave propagation in cased borehole models including single casing and dual casing boreholes with different bonding conditions. Pressure snapshots give us a direct way to evaluate wave excitations and propagation for different models. Data processing methods such as velocity-time semblance and dispersion analysis facilitate the identification of the modes in the different models. Modal decomposition gives us further insight into the waves present when the source is eccentered. Our conclusions are as follows:

(1) For single casing models, the formation modes can be easily discerned when the casing is well bonded. However, the P wave is submerged in the casing mode and the S wave has poor coherence when the cement is replaced with fluid. Acoustic logging tools having a monopole sonic source can be used to determine the bonding condition of different interfaces for the single casing model.

(2) For dual casing models, it is easy to distinguish the cases where there is good cement in both annuli or good cement in only the inner annulus from other cases by using monopole logging data. If the first annulus is not bonded well, it is possible to use dipole or higher order modes to distinguish the bonding condition.

(3) Modal decomposition method of the data helps us understand higher order modes that are generated when the source is eccentered.

Further work needs to be done in order to understand the full effect of eccentered pipes and sources to further evoluve the data processing methods.

ACKNOWLEDGEMENTS

This study was supported by STATOIL.

REFERENCES

Byun, J., M. N. Toksöz, 2003, Analysis of the acoustic wavefields excited by the Logging-While-Drilling (LWD) tool: Geosytem Eng., 6(1), 19-25.

Chen, T., Wang, B., Zhu, Z., and Burns, D., 2010, Asymmetric source acoustic LWD for improved formation shear velocity estimation: SEG Technical Program Expanded Abstracts, 548-552.

Kimball, C.V., T. Marzetta, 1986, Semblance processing of borehole acoustic array data: Geophysics, 49:274-281.

Lecampion B., Quesada D., Loizzo M., Bunger A., Kear J., Deremble L., Desroches J. (2011), Interface debonding as a controlling mechanism for loss of well integrity: Importance for CO2 injector wells, Energy Procedia, 4, 5219-5226.

Paillet, F., and C. H., Cheng, 1991, Acoustic waves in boreholes, P.154, CRC Press.

Plona, T., B. K., Sinha, S., Kostek, and S. K., Chang, 1992, Axisymmetric wave propagation in fluid-loaded cylindrical shells. II: Theory versus experiment, J. Acoust. Soc. Am., 92(2): 1144-1155.

Tubman, K. M., Cole, S. P., Cheng, C. H., Toksöz, M. N., 1984, Dispersion curves and synthetic microseismograms in unbonded cased boreholes, Earth Resources Laboratory Industry Consortia Annual Report, 1984-02.

Wang, H., G., Tao, and M. C., Fehler, 2015, Investigation of the high-frequency wavefield of an off-center monopole acoustic logging-while-drilling tool, GEOPHYSICS, 80(4): D329-D341.

Wang, H., G., Tao, X., Shang, 2016, Understanding acoustic methods for cement bond logging, J. Acoust. Soc. Am. 139(5), 2407-2416. DOI: 10.1121/1.4947511

Zhang, H., D., Xie, Z., Shang, X., Yang, H., Wang, H., Tao, Simulated various characteristic waves in acoustic full waveform relating to cement bond on the secondary interface, Journal of Applied Geophysics, 73, 139-154.

ABOUT THE AUTHORS

Hua Wang received his Ph.D. in exploration geophysics

from China University of Petroleum-Beijing in 2012. He was SEG scholarship recipient (2009, 2010, and 2011), founder and first President of Student Core Analyst Society of China University of Petroleum-Beijing during the Ph.D. period. After graduation he remained at China University of Petroleum-Beijing as a Postdoctoral Fellow. In May of 2014 he joined the Department of Earth, Atmospheric, and Planetary Sciences at MIT as a Postdoctoral Fellow. He is associate editor of Journal of Petroleum Science and Engineering, and Journal of Natural Gas Science and Engineering. The majority of his work has been dedicated to borehole geophysics, micro-seismicity induced by fluid injection in oil/gas exploration and geothermal exploitation, and exploration seismology. He may be contacted by E-mail at wanghuaupc@126.com.

Michael Fehler received his Ph.D. in seismology from MIT in 1979. After spending a few years in the College of Oceanography at Oregon State University, he joined Los Alamos National Laboratory in 1984 where he was leader of the Geophysics Group and later the Division Director of the Earth and Environmental Sciences Division that consisted of approximately 350 staff. He is currently a Senior Research Scientist in the Department of Earth, Atmospheric, and Planetary Sciences at Massachusetts Institute of Technology. He was Project Manager for the Phase I portion of the SEG Advanced Modeling project and he is now Project Manager of a SEAM project that focuses on predrill pore pressure prediction, He was Editor-in-Chief of the Bulletin of the Seismological Society of America for nine years beginning in 1995 and was president of the Seismological Society of America from 2005-2007. He has coauthored a book on seismic wave propagation and scattering that was published in 1998. A second edition of the book was completed and published in 2012.

Douglas Miller received his Ph.D. in Mathematics from the University of California at Berkeley in 1976. After teaching mathematics at Yale University and at the University of Illinois in Chicago, he joined the professional staff at Schlumberger-Doll Research in Ridgefield CT in 1981. Retired from Schlumberger after a 29 year career at research labs in Ridgefield CT, Cambridge UK, and Cambridge MA, he is a Research Affiliate at MIT's Earth Resources Laboratory and Principal Scientist at Miller Applied Science LLC. He has published work on a broad range of topics in applied mathematics and geophysics, focusing on the relation between measurements, mathematical models, and data analysis. A compendium of his work can be found at www.mit.edu

Ioan - Alexandru Merciu, is senior researcher at Statoil ASA, with responsibilities on logging and data analyze technologies development. Before assuming his current role, Alex was a Professional Field Engineer at Schlumberger Wireline leading and managing exploration wireline specific activities on international grounds with focus on Barents Sea and Norwegian Continental Shelf. Alex responsibilities containd all aspects of wireline operations. He has received Engineer Diplom. / MSc. in Applied Geophysics from University of Bucharest from 2004.